

Quantitative analysis of angle-resolved XPS spectra recorded in parallel data acquisition mode

M. S. Vinodh and L. P. H. Jeurgens*

Max Planck Institute for Metals Research, Heisenbergstraße 3, D-70569, Stuttgart, Germany

Received 18 August 2004; Revised 29 September 2004; Accepted 30 September 2004

The effects of anisotropy of the photoionization cross-section and elastic scattering of photoelectrons in solids are investigated for angle-resolved XPS spectra (ARXPS) recorded from α -Al₂O₃ substrate in parallel data acquisition mode. It is shown that for quantitative analysis of ARXPS spectra recorded in parallel data acquisition mode it is essential to account for the anisotropies of the photoionization cross-sections of the detected photoelectrons for the concerned elements in the solid due to variation of the angle between the incident x-rays and the detected photoelectrons. Neglecting the effect of elastic scattering only leads to minor errors in quantitative analysis of the ARXPS spectra. By adopting experimentally determined values for the relative sensitivity factors of the concerned photoelectrons in the solid as a function of the detection angle, cumbersome corrections for the effects of anisotropy of the photoionization cross-section and elastic scattering can be avoided. Copyright © 2004 John Wiley & Sons, Ltd.

KEYWORDS: angle-resolved XPS; parallel data acquisition; quantitative analysis; anisotropy of photoionization; asymmetry parameter; elastic scattering

INTRODUCTION

In a conventional XPS instrumental set-up, angle-resolved x-ray photoelectron spectroscopy (ARXPS) measurements are performed by tilting the specimen, thereby maintaining a fixed angle ψ between the incident x-rays and the analyser (i.e. the detected electrons; see Fig. 1). In general, the angle ψ is chosen to be close to 54°, corresponding to the so-called 'magic angle'. At this specific angle of ψ , the effect of anisotropy of the photoionization cross-section on the recorded photoelectron intensity cancels out and thus the *total* photoionization cross-section σ for the detected photoelectrons of the concerned elements in the solid can be used directly for quantification (see next section and Refs 1–3). The total photoionization cross-section σ_{AX_n} is defined as the transition probability (per unit time) for exciting a photoelectron from the n th subshell of core-level shell X of element A in the solid per unit incident photon flux.

The Thermo VG 'Thetaprobe' instrument employed in the present investigation has the capability of detecting photoelectrons over a wide angular range without tilting the sample (so-called parallel data acquisition mode), which greatly speeds up the recording of a series of ARXPS spectra. Further advantages compared with a conventional ARXPS set-up are that the analysed area and position remain constant, i.e. they are independent of the photoelectron detection angle α (with respect to the sample surface normal; see Fig. 1).

For an ARXPS measurement recorded in parallel data acquisition mode, the solid angle of acceptance of the analyser is divided into numerous channels, with each channel corresponding to a particular angular detection range (with a maximum possible 96 channels divided over a total detection range of $\alpha = 23$ –83° in the present case). This implies that, in contrast to a conventional XPS set-up, the angle ψ between the incident x-rays and detected photoelectrons is not a constant but varies with the detection angle α (see Fig. 1). As demonstrated in the present study, accurate quantitative analysis of these ARXPS spectra then requires knowledge of the anisotropy of the photoionization cross-section for each core-level photoelectron line studied (see next section). This implies that instead of the *total* photoionization cross-section σ , as used in the quantification of conventional ARXPS measurements, the *differential* photoionization cross-section $d\sigma/d\Omega$ of the elements in the solid must be employed in the quantification. The differential photoionization cross-section describes the angular distribution of the emitted photoelectrons as a function of solid acceptance angle, and its value depends on the angle ψ between the directions of the incident x-rays and the detected photoelectrons, the orbital angular quantum number and kinetic energy of the concerned photoelectrons (see next section).

The present study investigates the effects of the anisotropy of the photoionization cross-section and elastic scattering of the emitted photoelectrons in the solid on the quantitative analysis of ARXPS spectra recorded in parallel data acquisition mode. As a case study, the relative sensitivity factor (S) for the O 1s to Al 2p photoemission process in α -Al₂O₃ as a function of the angles α and ψ is determined

*Correspondence to: L. P. H. Jeurgens, Max Planck Institute for Metals Research, Heisenbergstrasse 3, D-70569, Stuttgart, Germany. E-mail: l.p.h.jeurgens@mf.mpg.de

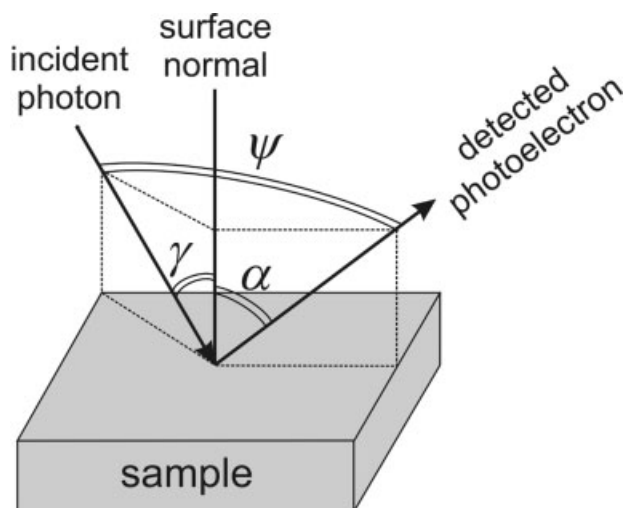


Figure 1. Schematic illustration of the interaction of incident photons with the sample surface: γ is the angle between the directions of the incident photon and the sample surface normal; α is the detection angle between the directions of the detected photoelectron and the sample surface normal; and ψ is the angle between the directions of the incident photon and the detected photoelectron.

from their corresponding ARXPS spectra recorded in parallel data acquisition mode. Such experimentally determined sensitivity factors (S) for various angles α and ψ can be employed to calculate the composition, film thickness or depth distributions of various oxidic species, e.g. in thin oxide films grown on metal substrates by thermal oxidation (cf. Ref. 4). The results will provide a framework for the interpretation of ARXPS spectra as recorded with state-of-the-art ARXPS instruments employing parallel data acquisition mode.

In the next section the theory on the anisotropy of the photoionization cross-section and the correction factors involved in quantification of ARXPS spectra (with and without accounting for the effects of elastic scattering) are presented. Also, a simple method for the determination of relative sensitivity factors from measured ARXPS spectra is given. The experimental details and the data evaluation procedure are given and, finally, the results and discussion are presented in terms of the effects of the anisotropies of the photoionization cross-sections and elastic scattering on the relative O 1s to Al 2p sensitivity factor determined from the ARXPS measurement of α -Al₂O₃ (in parallel data acquisition mode).

THEORY

The observed primary zero-loss (PZL) intensity $I_{AX_n}^\infty$ (cf. Ref. 5) of photoelectrons ejected with a kinetic energy E from the n th subshell of core-level shell X of an element A distributed within a solid can be expressed by (cf. Ref. 6)

$$I_{AX_n}^\infty = K \left(d\sigma_{AX_n}/d\Omega \right) \int_{z=0}^{\infty} C_A(z) \times \exp \left[- \int_{z'=0}^z \frac{dz'}{\lambda_{AX_n}^i(z', E) \cos \alpha} \right] dz \quad (1)$$

where: K is an instrumental factor that depends on factors such as area of analysis, energy and flux of the incident x-rays and solid acceptance angle of the analyser (cf. Ref. 6); detection angle α is defined as the angle between the specimen surface normal and the solid acceptance angle of the analyser (see Fig. 1); $C_A(z)$ is the atomic density of element A in the solid as a function of depth z below the sample surface; $\lambda_{AX_n}^i(z, E)$ is the inelastic mean free path (IMFP) of the detected photoelectrons traversing with kinetic energy E through the solid as a function of depth z below the sample surface; and $(d\sigma_{AX_n}/d\Omega)$ is the differential photoionization cross-section. The depth dependence of IMFP due to possible changes in composition (as experienced for thin metal oxide film systems when proceeding from the substrate to the oxide film, cf. Ref. 6) is accounted for by the second integral over dz' . In Eqn. (1) the effect of elastic scattering of the photoelectrons propagating through the solid has been neglected.

Anisotropy of photoionization cross-section

The differential photoionization cross-section $(d\sigma_{AX_n}/d\Omega)$ obtained in the dipole approximation (cf. p. 42 in Ref. 1) for unpolarized x-rays and a randomly oriented set of atoms (or molecules) in the solid, as appropriate to studies of gaseous, polycrystalline or amorphous specimens, is expressed by (cf. Refs 2 and 3)

$$(d\sigma_{AX_n}/d\Omega) = \sigma_{AX_n} W(\psi, \beta_{AX_n}) = \frac{\sigma_{AX_n}}{4\pi} \left[1 - \frac{\beta_{AX_n}}{4} (3 \cos^2 \psi - 1) \right] \quad (2)$$

where: σ_{AX_n} is the total photoionization cross-section (integrated over the full 4π range for a given angle ψ between the directions of the incident photon beam and the ejected photoelectrons; see Fig. 1), defined as the transition probability (per unit time) of emitting a photoelectron from the n th subshell of core-level X of element A in the solid per unit incident photon flux; $W(\psi, \beta_{AX_n})$ is the asymmetry factor describing the intrinsic anisotropy of the photoionization cross-section; and β_{AX_n} is the asymmetry parameter describing the angular distribution of the ejected photoelectrons concerned.

The allowed range for the asymmetry parameter β_{AX_n} is determined by the requirement that the cross-section should be non-negative (cf. Ref. 1), i.e. $-1 \leq \beta_{AX_n} \leq 2$. A positive value of β_{AX_n} implies that photoelectrons are preferentially emitted at angles perpendicular to the direction of the incident photons (i.e. $\psi = 90^\circ$), whereas a negative value indicates preferential emission parallel or anti-parallel to this direction (i.e. $\psi = 0^\circ$ or 180°). A value of $\beta_{AX_n} = 0$ yields an isotropic distribution. The exact value of β_{AX_n} depends upon the orbital angular momentum quantum number l (i.e. the type of subshell) and the kinetic energy of the emitted photoelectrons (and thus on the incident photon energy $h\nu$), where for all s-type subshells (i.e. $l = 0$) the value of $\beta_{AX_n} = 2$. Values of β_{AX_n} are tabulated in the literature only for elements in their gas phase (cf. Refs 7–9).

As follows from Eqn. (2), due to the anisotropy of the photoionization cross-section the recorded photoelectron intensity depends on the angle ψ between the directions of the incident photons and the detected photoelectrons (see Fig. 1). In a conventional XPS set-up, the x-ray source and

the analyser are fixed and the angle between them is usually chosen close or equal to the so-called magic angle of $\psi = 54.74^\circ$, for which the β -dependent term on the right-hand side of Eqn. (2) vanishes. In this case, even for angle-resolved measurements (obtained as a function of the detection angle α for a fixed angle of ψ by tilting the sample; see Fig. 1), no correction for the anisotropy of the photoionization cross-section $W(\psi, \beta_{AX_n})$ is required upon quantification. This implies that only the total photoionization cross-section is required for the quantification of these ARXPS spectra.

On the other hand, for a state-of-the-art ARXPS measurement employing parallel data acquisition mode, the signal intensities are collected simultaneously over a wide range of detection angle α , while fixing both the sample position and the angle γ between the incident photon beam and the sample normal (see Fig. 1). Consequently, the angle ψ does vary with the detection angle α , and separate values of $W(\psi, \beta_{AX_n})$ are required upon quantification for each detection angle concerned (see Results and Discussion).

Effect of elastic scattering

Elastic scattering of emitted photoelectrons in a solid affects the distribution of the photoelectron trajectories, i.e. it partially randomizes the direction of electron motion. Consequently, the *observed* anisotropy of the differential photonization cross-section of an element in the solid differs from the corresponding *intrinsic* anisotropy of the differential photonization cross-section of the isolated atom; i.e. the anisotropy observed for solids is a little less pronounced (the asymmetry parameter β_{AX_n} is relatively lower). The results of Monte-Carlo (MC) simulations (cf. Refs 10 and 11) have shown that the effect of elastic scattering in solids can be accounted for by replacing the cross-section ($d\sigma_{AX_n}/d\Omega$) of Eqn. (1) with an effective differential photonization cross-section, defined as

$$(d\sigma_{AX_n}/d\Omega)_{\text{eff}} = \sigma_{AX_n} W(\psi, \beta_{AX_n}^{\text{eff}}) = \sigma_{AX_n} Q_{AX_n} \frac{1}{4\pi} \left[1 - \frac{\beta_{AX_n}^{\text{eff}}}{4} (3 \cos^2 \psi - 1) \right] \quad (3a)$$

where $\beta_{AX_n}^{\text{eff}}$ denotes the effective asymmetry parameter describing the actual, observed angular distribution of the measured photoelectron intensities, and Q_{AX_n} is a weak correction factor (ranging between 0.9 and 1) accounting for the reduction in the overall escape probability of photoelectrons due to elastic scattering within the solid (i.e. it describes the relative change in the observed photoelectron intensities due to elastic collisions). The incorporation of $(d\sigma_{AX_n}/d\Omega)_{\text{eff}}$ in Eqn. (1) is equivalent to replacing the IMFP in Eqn. (1) (i.e. $\lambda_{AX_n}^i$) by an effective attenuation length (EAL) $\lambda_{AX_n}^{\text{eff}}$, defined as (cf. Ref. 12)

$$\lambda_{AX_n}^{\text{eff}} = \lambda_{AX_n}^i Q_{AX_n} \frac{W(\psi, \beta_{AX_n}^{\text{eff}})}{W(\psi, \beta_{AX_n})} \quad (3b)$$

Accurate expressions for the parameters Q_{AX_n} and $\beta_{AX_n}^{\text{eff}}$ obtained within the so-called transport approximation, which neglects the structure in the differential elastic

scattering cross-sections (i.e. isotropic elastic scattering is assumed), are given by (cf. Ref. 13)

$$Q_{AX_n} = (1 - \omega)(D_1 + D_2) \quad (4a)$$

and

$$\beta_{AX_n}^{\text{eff}} = (1 - \omega) \frac{\beta_{AX_n}}{Q_{AX_n}} \quad (4b)$$

where

$$D_1 = \frac{H(\cos \alpha, \omega)}{\sqrt{(1 - \omega)}} \quad (4c)$$

and

$$D_2 = \frac{\omega \beta_{AX_n}}{16} (3 \cos^2 \psi - 1) H(\cos \alpha, \omega) \times \int_0^1 x H(x, \omega) (x + \cos \alpha)^{-1} (3x^2 - 1) dx \quad (4d)$$

In the above equations, ω is the so-called single scattering albedo defined as

$$\omega = \left[1 + \frac{\lambda_{AX_n}^{\text{tr}}}{\lambda_{AX_n}^i} \right]^{-1} \quad (5a)$$

where $\lambda_{AX_n}^{\text{tr}}$ denotes the transport mean free path (TMFP) of the concerned photoelectrons of kinetic energy E in the solid, which for a solid compound consisting of m components is given by (cf. Ref. 14)

$$\lambda_{AX_n}^{\text{tr}} = \left(M \sum_{k=1}^m x_k \sigma_{\text{tr},k} \right)^{-1} \quad (5b)$$

Here, M is the total atomic density of the compound, x_k is the atom fraction of the k th component in the compound and $\sigma_{\text{tr},k}$ represents the transport scattering cross-section of the k th component for the concerned photoelectrons with kinetic energy E (cf. Ref. 14). Finally, the term $H(\cos \alpha, \omega)$ in Eqns 4(c) and 4(d) is the Chandrasekhar function (Ref. 15), which can be solved by an iterative procedure (see Ref. 15) (a matlab script to solve the function of Chandrasekhar, $H(x, \omega)$, for any value of $0 \leq x \leq 1$ and $0 \leq \omega \leq 1$ by an iterative procedure can be obtained upon request from the author) or approximated by an analytical expression (cf. Ref. 12).

The term D_2 in Eqn. (4a) is generally neglected, because its value in all cases is considerably smaller than the value for the D_1 term (cf. Refs 12 and 13). Further, it is noted that for pure elements, simpler approximate expressions for the estimation of factors Q_{AX_n} and $\beta_{AX_n}^{\text{eff}}$ are reported in the literature (cf. Ref. 16).

Relative sensitivity factor in binary solids

Adopting Eqns (1), (2) and (3b), it follows that the composition (i.e. the atomic ratio) of a homogeneous, infinitely thick (as compared to the IMFP) binary compound AB is related to the measured total PZL photoelectron intensities $I_{AX_n}^\infty$ and $I_{BY_m}^\infty$ recorded from elements A and B in the solid by

$$\frac{C_A}{C_B} = \frac{I_{AX_n}^\infty}{I_{BY_m}^\infty} \cdot \frac{\lambda_{BY_m}^{\text{eff}}}{\lambda_{AX_n}^{\text{eff}}} \cdot \frac{\sigma_{BY_m} W(\psi, \beta_{BY_m})}{\sigma_{AX_n} W(\psi, \beta_{AX_n})} = \frac{I_{AX_n}^\infty}{I_{BY_m}^\infty} \cdot \frac{\lambda_{BY_m}^i}{\lambda_{AX_n}^i} \cdot \frac{\sigma_{BY_m}}{\sigma_{AX_n}} \cdot \frac{Q_{BY_m} W(\psi, \beta_{BY_m}^{\text{eff}})}{Q_{AX_n} W(\psi, \beta_{AX_n}^{\text{eff}})} \quad (6a)$$

where $I_{AX_n}^\infty$ and $I_{BY_m}^\infty$ denote the PZL intensities of the photoelectrons emitted from the n th and m th subshells of core-level shells X and Y of elements A and B within the (infinitely thick) solid, respectively. The relative sensitivity factor S_{AX_n/BY_m} for the AB reference compound with a known atomic ratio C_A/C_B is then defined as

$$S_{AX_n/BY_m} = \frac{C_B}{C_A} \cdot \frac{I_{AX_n}^\infty}{I_{BY_m}^\infty} = \frac{\lambda_{AX_n}^{\text{eff}}}{\lambda_{BY_m}^{\text{eff}}} \cdot \frac{\sigma_{AX_n} W(\psi, \beta_{AX_n})}{\sigma_{BY_m} W(\psi, \beta_{BY_m})} \\ = \frac{\lambda_{AX_n}^i}{\lambda_{BY_m}^i} \cdot \frac{\sigma_{AX_n}}{\sigma_{BY_m}} \cdot \frac{Q_{AX_n} W(\psi, \beta_{AX_n}^{\text{eff}})}{Q_{BY_m} W(\psi, \beta_{BY_m}^{\text{eff}})} \quad (6b)$$

Consequently, the relative sensitivity factor incorporates the combined effects of:

- (1) The relative difference in the EALs $\lambda_{AX_n}^{\text{eff}}$ and $\lambda_{BY_m}^{\text{eff}}$ as a function of angles α and ψ (i.e. the relative difference in inelastic and elastic scattering of the concerned photoelectrons during their transport through the solid).
- (2) The relative difference in the total photoionization cross-sections σ_{AX_n} and σ_{BY_m} (independent of α and ψ).
- (3) The relative difference in the asymmetry factors $W(\psi, \beta_{AX_n})$ and $W(\psi, \beta_{BY_m})$ as a function of angle ψ (i.e. the relative difference in the anisotropy in the angular distribution of the concerned photoelectrons).

As follows from Eqn. (6b), the value for S_{AX_n/BY_m} as a function of angle ψ and/or detection angle α (see Fig. 1) can be determined experimentally from the PZL intensity ratio $I_{AX_n}^\infty/I_{BY_m}^\infty$ obtained from a series of measured XPS spectra recorded from the reference compound for a various set of ψ and α angles.

In a conventional XPS set-up (for which angle ψ is fixed for various detection angles α ; see section on anisotropy of photoionization cross-section), the experimentally obtained value of S_{AX_n/BY_m} should be independent of the detection angle α provided that the EAL ratio $\lambda_{AX_n}^{\text{eff}}/\lambda_{BY_m}^{\text{eff}}$ is a constant and no photoelectron diffraction effects occur (as is valid for polycrystalline and amorphous solids). Moreover, if such a series of measurements is made at the magic angle of ψ , the asymmetry factor ratio in Eqn. (6b) vanishes (see Theory).

On the other hand, for a similar ARXPS measurement employing parallel data acquisition mode (for which angle ψ varies with detection angle α ; see section on anisotropy of photoionization cross-section), S_{AX_n/BY_m} does depend upon the detection angle α due to the accompanied change in angle ψ (see Fig. 1). Only for the special case where both subshells n and m are of the s-type (i.e. $\beta_{AX_n} = \beta_{AY_m} = 2$) is the experimentally obtained value of S_{AX_n/BY_m} independent of the detection angle α (again, provided that $\lambda_{AX_n}^{\text{eff}}/\lambda_{BY_m}^{\text{eff}}$ is a constant and no photoelectron diffraction effects occur).

Knowledge of the dependence of the value of S_{AX_n/BY_m} on angles ψ and α is required for the quantification of ARXPS spectra recorded from binary compounds of unknown composition, as well as from thin layered structures on substrates (as, for example, in the determination of thicknesses and compositions of thin oxide films on metal substrates; cf. Ref. 4). In the next section, the variation of the relative sensitivity factor $S_{O1s/Al2p}$ with the interdependent angles ψ and α will be investigated for the ARXPS spectra recorded in parallel data

acquisition mode from an $\alpha\text{-Al}_2\text{O}_3$ reference with a known O/Al atomic ratio of 1.5. The values of $S_{O1s/Al2p}$ obtained as a function ψ and α may be adopted in the quantification of ARXPS spectra recorded from thin Al oxide films grown on Al substrates by thermal oxidation (cf. Ref. 4).

EXPERIMENTAL AND DATA EVALUATION

A one-side-polished ($<0.25\ \mu\text{m}$) (1100)-oriented $\alpha\text{-Al}_2\text{O}_3$ single crystal with an O/Al ratio of 1.5 (purity $<99.99\%$ supplied by Goodfellow Cambridge Ltd) was thoroughly cleaned ultrasonically in acetone, ethanol and 2-propanol and then dried by blowing with pure compressed nitrogen gas. Next, the sample was introduced into an ultrahigh vacuum chamber at a base pressure of $<3 \times 10^{-8}$ Pa, for XPS analysis. First, the adventitious carbon and any other contaminants present on the oxide surface were removed by a short (a few minutes) gentle sputter-cleaning treatment with low-energy (1 kV) Ar^+ ions. After this sputter-cleaning treatment, no surface contaminants were detected in the XPS spectra recorded over a binding energy (BE) range of 0–1400 eV (see below for instrumental details).

The ARXPS analysis of the specimen was performed with a Thermo VG Thetaprobe system operating in the so-called parallel data acquisition mode (see introduction) using monochromatic incident Al $K\alpha$ radiation ($h\nu = 1486.68$ eV; spot size $400\ \mu\text{m}$). The emitted electrons were detected simultaneously over the angular range (with respect to the surface normal) of $23\text{--}83^\circ$ in eight ranges of 7.5° each. The energy scale of the concentric hemispherical analyser (CHA) was calibrated with high-purity, sputter-cleaned reference samples of Au, Ag and Cu, such that the corresponding Au $4f_{7/2}$, Ag $3d_{5/2}$ and Cu $2p_{3/2}$ main peaks were positioned at the recommended BE values of 83.98, 368.26 and 932.67 eV, respectively.¹⁷

The survey spectra were recorded in the BE range 0–1400 eV at a constant pass energy of 100 eV and step size of 0.1 eV. The angle-resolved spectra of Al 2p and O 1s photoelectron lines were measured in the BE ranges 65–80 and 525–540 eV, respectively, with a pass energy of 100 eV and a step size of 0.1 eV.

Charge compensation of the insulating $\alpha\text{-Al}_2\text{O}_3$ specimen during the XPS analysis was achieved by irradiation of the sample surface with a diffuse beam of low-energy electrons (kinetic energy = 3 eV; emission current $\sim 35\ \mu\text{A}$) using a flood gun equipped with an LaB₆ cathode. The flood gun was operated at the lowest possible temperature (~ 1200 K) to minimize the thermal energy spread within the incident electron beam. Optimum charge compensation was achieved by tuning the flood gun settings to obtain the most symmetrical and narrow-shaped oxidic Al 2p main peak possible from the insulating $\alpha\text{-Al}_2\text{O}_3$ specimen.

The averaged value (and corresponding standard deviation for the ARXPS spectra recorded at the various emission angles; see above) for the BE position and full width at half-maximum (FWHM) of the oxidic Al 2p main peaks of the $\alpha\text{-Al}_2\text{O}_3$ reference correspond to 70.52 ± 0.05 and 1.86 ± 0.05 eV, respectively. The corresponding values for the BE position and FWHM of the O 1s main peak of

the $\alpha\text{-Al}_2\text{O}_3$ reference are 527.27 ± 0.04 and 2.16 ± 0.12 eV, respectively. This results in an average value (and standard deviation) for the Al–O binding state parameter $E_{\text{Al-O}}$ (O 1s BE—Al 2p BE) for $\alpha\text{-Al}_2\text{O}_3$ of 456.75 ± 0.02 eV. Note that the value of $E_{\text{Al-O}}$ is independent of the incident photon energy, reference level and charging effects (cf. Ref. 4). The value of $E_{\text{Al-O}}$ obtained for $\alpha\text{-Al}_2\text{O}_3$ in the present study is in excellent agreement with the corresponding value of 456.76 eV reported in Ref. 18.

The total PZL intensities (cf. Ref. 5) of the oxidic Al 2p and O 1s main peaks as a function of detection angle α were resolved from the corresponding ARXPS spectra recorded from the $\alpha\text{-Al}_2\text{O}_3$ reference as follows. First, all measured Al 2p and O 1s spectra were corrected for the electron kinetic energy-dependent transmission of the hemispherical analyser of the spectrometer by adopting the corresponding correction factor as provided by the manufacturer (see above). Next, the relatively small background of inelastically scattered electrons in the BE regions of the Al 2p and O 1s main peaks was removed by subtraction of a Shirley-type background in the BE ranges of the main peaks i.e. 69–79 and from 525–538 eV, respectively. The total oxidic Al 2p and O 1s PZL intensities were taken to be equal to the integrated area under the corresponding background-corrected main peaks.

RESULTS AND DISCUSSION

The O 1s to Al 2p relative sensitivity factor (RSF) $S_{\text{O1s/Al2p}}$ for the $\alpha\text{-Al}_2\text{O}_3$ reference is defined as (see section on RSF in binary solids)

$$S_{\text{O1s/Al2p}} = \frac{2}{3} \cdot \frac{I_{\text{O1s}}^{\infty}}{I_{\text{Al2p}}^{\infty}} = \frac{\lambda_{\text{O1s}}^{\text{eff}}}{\lambda_{\text{Al2p}}^{\text{eff}}} \cdot \frac{\sigma_{\text{O1s}} W(\psi, \beta_{\text{O1s}})}{\sigma_{\text{Al2p}} W(\psi, \beta_{\text{Al2p}})}$$

$$= \frac{\lambda_{\text{O1s}}^{\text{i}}}{\lambda_{\text{Al2p}}^{\text{i}}} \cdot \frac{\sigma_{\text{O1s}}}{\sigma_{\text{Al2p}}} \cdot \frac{Q_{\text{O1s}} W(\psi, \beta_{\text{O1s}}^{\text{eff}})}{Q_{\text{Al2p}} W(\psi, \beta_{\text{Al2p}}^{\text{eff}})} \quad (7)$$

The value of $S_{\text{O1s/Al2p}}$ determined from the total Al 2p and O 1s PZL intensities resolved from the measured ARXPS spectra of the $\alpha\text{-Al}_2\text{O}_3$ specimen (and adopting the known Al/O atomic ratio of 2:3) is plotted as a function of detection angle α and angle ψ in Fig. 2. Note that because the ARXPS measurements were recorded in parallel data acquisition mode, a change in detection angle α is accompanied by a corresponding change in angle ψ between the directions of the incident x-ray beam and the detected photoelectrons (see Introduction).

Evidently, the values of $S_{\text{O1s/Al2p}}$ obtained increase with an increase of the interdependent angles α and ψ , i.e. the value for $S_{\text{O1s/Al2p}}$ is at a maximum (minimum) for the grazing (near-normal) angles of α with respect to the sample surface, corresponding to a large (small) ψ between the directions of the incident x-ray beam and the detected photoelectrons (see Fig. 1). Note that for a similar series of ARXPS measurements performed in a conventional XPS set-up (i.e. ψ is a constant fixed at the magic angle, and detection angle α is varied by tilting the sample), the RSF $S_{\text{O1s/Al2p}}$ would be independent of the detection angle α (in the absence of elastic electron scattering and photoelectron diffraction effects within the solid; see Theory section).

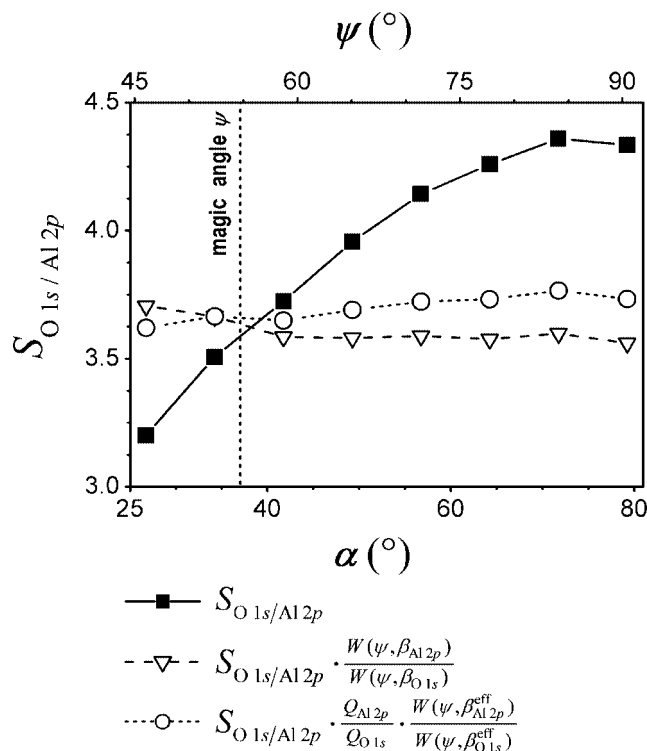


Figure 2. The relative sensitivity factor (RSF) $S_{\text{O1s/Al2p}}$ for $\alpha\text{-Al}_2\text{O}_3$ versus interdependent angles α (bottom x-axis) and ψ (top x-axis) (see Fig. 1). The terms $S_{\text{O1s/Al2p}}[W(\psi, \beta_{\text{Al2p}})/W(\psi, \beta_{\text{O1s}})]$ and $S_{\text{O1s/Al2p}} \left\{ Q_{\text{Al2p}}/Q_{\text{O1s}} [W(\psi, \beta_{\text{Al2p}}^{\text{eff}})/W(\psi, \beta_{\text{O1s}}^{\text{eff}})] \right\}$ are also plotted as a function of interdependent angles α and ψ (see text for details).

As discussed, the observed change in the RSF with the interdependent angles α and ψ (in parallel data acquisition mode) is due to the combined effects of the anisotropies of the photoionization cross-sections and the elastic scattering of the detected photoelectrons within the solid. In this case, the relative difference between the intrinsic anisotropies of the Al 2p and O 1s photoionization cross-sections is expressed in Eqn. (7) by the asymmetry factor ratio $W(\psi, \beta_{\text{O1s}})/W(\psi, \beta_{\text{Al2p}})$, the value of which depends only upon the angle ψ (see Eqn. (3a)). The relative difference in elastic (and inelastic) scattering of the detected O 1s and Al 2p photoelectrons within the solid, on the other hand, is expressed in Eqn. (7) by the EAL ratio $\lambda_{\text{O1s}}^{\text{eff}}/\lambda_{\text{Al2p}}^{\text{eff}}$, the value of which depends mainly on the detection angle α (due to the dependence of the corresponding Q factors on the angle α ; see Eqns (4a)–(4d)).

To investigate the effect of the intrinsic anisotropies of the Al 2p and O 1s photoionization cross-sections on the angular dependence of the RSF, the value of $S_{\text{O1s/Al2p}}$ is divided by the asymmetry factor ratio $W(\psi, \beta_{\text{O1s}})/W(\psi, \beta_{\text{Al2p}})$ (see Eqn. (7)) and plotted as a function of the interdependent angles α and ψ in Fig. 2. All data used for calculation of asymmetry factors $W(\psi, \beta_{\text{O1s}})$ and $W(\psi, \beta_{\text{Al2p}})$ (using the appropriate expressions given in the Theory section), as well as their resulting values, are reported in Tables 1 and 2, respectively. Evidently, the value of $S_{\text{O1s/Al2p}}[W(\psi, \beta_{\text{Al2p}})/W(\psi, \beta_{\text{O1s}})]$ is nearly constant over the angular detection range of 40–80° (corresponding to a ψ range of 56–91°). This implies that

Table 1. Physical constants used for calculations of the effective asymmetry parameters (β^{eff}), the Q factors and the effective attenuation lengths (λ^{eff})

Constant	Value	Units	Ref.
Density of $\alpha\text{-Al}_2\text{O}_3$	3.99×10^6	g m^{-3}	19
Molecular mass of $\alpha\text{-Al}_2\text{O}_3$	101.961	g mol^{-1}	
Bandgap of $\alpha\text{-Al}_2\text{O}_3$	8.7	eV	
Asymmetry factor:			7
$\beta_{\text{Al}2p}$	0.93		
$\beta_{\text{O}1s}$	2.00		
Kinetic energy: Al 2p photoelectrons	1416.16	eV	20
O 1s photoelectrons	954.41	eV	
Inelastic mean free path:			
$\lambda_{\text{Al}2p}^i$	3.257	nm	21
$\lambda_{\text{O}1s}^i$	2.416	nm	
Transport cross-sections:			
$\sigma_{\text{tr,Al}}(\text{KE} = 1416.16 \text{ eV})$	6.93×10^{-22}	m^2	21
$\sigma_{\text{tr,O}}(\text{KE} = 1416.16 \text{ eV})$	3.25×10^{-22}	m^2	
$\sigma_{\text{tr,Al}}(\text{KE} = 954.41 \text{ eV})$	12.49×10^{-22}	m^2	
$\sigma_{\text{tr,O}}(\text{KE} = 954.41 \text{ eV})$	6.13×10^{-22}	m^2	
Transport Mean Free Path:			
$\lambda_{\text{Al}2p}^{\text{tr}}$	17.98	nm	
$\lambda_{\text{O}1s}^{\text{tr}}$	9.78	nm	
Single scattering albedo:			
$\omega_{\text{Al}2p}$	0.153		
$\omega_{\text{O}1s}$	0.198		

the variation of the RSF over this angular range is, to a first approximation, solely determined by the relative changes of the intrinsic anisotropies of the Al 2p and O 1s photoionization cross-sections with ψ .

Nevertheless, the value of $S_{\text{O}1s/\text{Al}2p}[W(\psi, \beta_{\text{Al}2p})/W(\psi, \beta_{\text{O}1s})]$ shows a small, but distinct, increase with decreasing angles for the near-normal detection range (i.e. within the ranges $25^\circ < \alpha < 40^\circ$ and $45^\circ < \psi < 56^\circ$; see Fig. 2), indicating that an additional factor is responsible for the variation of $S_{\text{O}1s/\text{Al}2p}$ within this angular range. To investigate whether the variation of the RSF within this near-normal detection range is to some extent caused by differences in elastic scattering of the detected Al 2p and O 1s photoelectrons, the

term $S_{\text{O}1s/\text{Al}2p} \left\{ (Q_{\text{Al}2p}/Q_{\text{O}1s}) [W(\psi, \beta_{\text{Al}2p}^{\text{eff}})/W(\psi, \beta_{\text{O}1s}^{\text{eff}})] \right\}$ (see Eqn. (7)) is plotted as a function of angles α and ψ in Fig. 2. All data used for calculation of the effective asymmetry factors and Q factors (using the appropriate expressions given in the Theory section), as well as their resulting values, are reported in Tables 1 and 2, respectively. Indeed, the value of $S_{\text{O}1s/\text{Al}2p} \left\{ (Q_{\text{Al}2p}/Q_{\text{O}1s}) [W(\psi, \beta_{\text{Al}2p}^{\text{eff}})/W(\psi, \beta_{\text{O}1s}^{\text{eff}})] \right\}$, which incorporates the combined effects of the anisotropies of the photoionization cross-sections and elastic scattering, is approximately constant over the near-normal detection range (i.e. $25^\circ < \alpha < 40^\circ$ and $45^\circ < \psi < 56^\circ$; see Fig. 2). This confirms that the variation of the RSF over this angular range is indeed, to some extent, also determined by differences in elastic scattering of the Al 2p and O 1s photoelectrons.

It should be noted that the value of the RSF in the grazing detection angle range of, say, $\alpha > 70^\circ$, will be affected by small deviations from stoichiometry at the $\alpha\text{-Al}_2\text{O}_3$ surface (due to preferential sputtering effects upon cleaning; see Experimental and Data Evaluation). On the other hand, even for 10% deviation in the oxide stoichiometry, the changes in the corresponding asymmetry- and Q factors are negligible.

As discussed earlier, the effect of elastic scattering of the detected photoelectrons on the observed PZL photoelectron intensity is two fold: it affects the intrinsic anisotropy of the photoionization cross-section, as described by the reduction of parameter β_{AX_n} to an effective asymmetry parameter $\beta_{\text{AX}_n}^{\text{eff}}$; and it affects the overall escape probability of the emitted photoelectrons, as described by the weak correction factor Q_{AX_n} . The separate contributions of these two elastic scattering parameters to the observed variation of the RSF $S_{\text{O}1s/\text{Al}2p}$ with α and ψ are expressed by the corresponding values of $Q_{\text{Al}2p}/Q_{\text{O}1s}$ and $[W(\psi, \beta_{\text{Al}2p}^{\text{eff}})/W(\psi, \beta_{\text{O}1s}^{\text{eff}})][W(\psi, \beta_{\text{O}1s})/W(\psi, \beta_{\text{Al}2p})]$. The values for these two terms are plotted as a function of angles α and ψ in Fig. 3. Clearly, their contributions to the resulting value of $S_{\text{O}1s/\text{Al}2p}$ are very small, i.e. up to 3%, with the effect of elastic scattering on the relative difference in anisotropies of the photoionization cross-sections (i.e. the term $[W(\psi, \beta_{\text{Al}2p}^{\text{eff}})/W(\psi, \beta_{\text{O}1s}^{\text{eff}})][W(\psi, \beta_{\text{O}1s})/W(\psi, \beta_{\text{Al}2p})]$) being more pronounced. Moreover, it can be concluded from Fig. 3 that the relative differences between the Al 2p and O 1s elastic scattering parameters (i.e. β^{eff} and Q), cancel out to some extent in the near-normal detection range

Table 2. Calculated values of the Chandrasekhar functions ($H(x, \omega)$; see Ref. 15), the effective asymmetry parameters (β^{eff}), the Q factors and the effective attenuation lengths (λ^{eff}) as a function of interdependent angles α and ψ (see Fig. 1)

α ($^\circ$)	ψ ($^\circ$)	$H(\cos \alpha, \omega_{\text{Al}2p})$	$H(\cos \alpha, \omega_{\text{O}1s})$	$\beta_{\text{Al}2p}^{\text{eff}}$	$\beta_{\text{O}1s}^{\text{eff}}$	$Q_{\text{Al}2p}$	$Q_{\text{O}1s}$	$\lambda_{\text{Al}2p}^{\text{eff}}$ (nm)	$\lambda_{\text{O}1s}^{\text{eff}}$ (nm)
26.75	45.86	1.0564	1.0751	0.8097	1.6639	0.9725	0.9639	3.2154	2.4438
34.25	51.71	1.0550	1.0732	0.8110	1.6682	0.9709	0.9615	3.1767	2.3544
41.75	57.84	1.0532	1.0706	0.8126	1.6736	0.9689	0.9584	3.1418	2.2889
49.25	64.17	1.0507	1.0673	0.8148	1.6803	0.9663	0.9546	3.1114	2.2408
56.75	70.62	1.0474	1.0629	0.8176	1.6886	0.9630	0.9498	3.0851	2.2050
64.25	77.16	1.0430	1.0569	0.8213	1.6992	0.9588	0.9439	3.0618	2.1779
71.75	83.75	1.0370	1.0488	0.8262	1.7131	0.9530	0.9362	3.0401	2.1563
79.25	90.37	1.0281	1.0370	0.8333	1.7326	0.9449	0.9257	3.0168	2.1367

Values are calculated from appropriate expressions as given in the text and employing the data listed in Table 1.

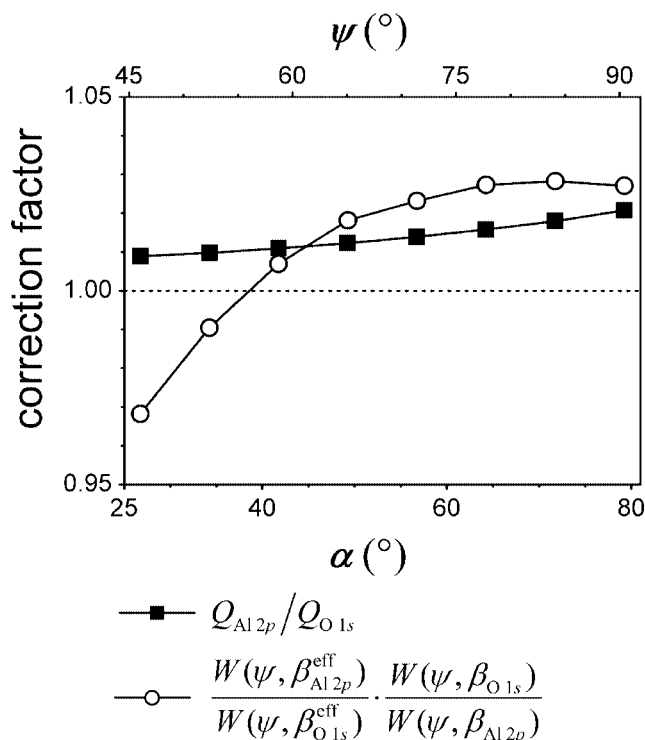


Figure 3. Calculated values of $[W(\psi, \beta_{\text{Al}2p}^{\text{eff}})/W(\psi, \beta_{\text{O}1s}^{\text{eff}})]$ $[W(\psi, \beta_{\text{O}1s})/W(\psi, \beta_{\text{Al}2p})]$ and $Q_{\text{O}1s}/Q_{\text{Al}2p}$ for $\alpha\text{-Al}_2\text{O}_3$ as a function of interdependent angles α (bottom x-axis) and ψ (top x-axis) (see Fig. 1). The term $[W(\psi, \beta_{\text{Al}2p}^{\text{eff}})/W(\psi, \beta_{\text{O}1s}^{\text{eff}})]$ $[W(\psi, \beta_{\text{O}1s})/W(\psi, \beta_{\text{Al}2p})]$ is a measure of the effect of elastic scattering on the anisotropy of the intrinsic photoionization cross-section, whereas the term $Q_{\text{O}1s}/Q_{\text{Al}2p}$ describes the effect of elastic scattering on the overall escape probability of the detected photoelectrons (see text for details).

(i.e. $25^\circ < \alpha < 40^\circ$ and $45^\circ < \psi < 56^\circ$). Consequently, the effect of elastic scattering on the *absolute* value of the relative sensitivity factor is more pronounced for detection angle $\alpha > 40^\circ$.

It can be concluded that, for recording of ARXPS spectra in parallel data acquisition mode the observed variation of the RSF with the interdependent angles α and ψ can be ascribed fully to the combined effects of the anisotropies of the photoionization cross-sections and the elastic scattering of the detected photoelectrons within the solid. For quantitative analysis of ARXPS spectra recorded in parallel data acquisition mode, it is therefore essential to apply the correct RSFs for each angular range concerned.

As an example, for the errors introduced in quantification when these effects are ignored, determination of the composition of the measured $\alpha\text{-Al}_2\text{O}_3$ reference (with a known O/Al ratio of 3:2) is considered (see Fig. 4). The composition of the measured oxide reference, expressed as the oxygen to metal ratio, is calculated from (cf. Eqn. (7))

$$\frac{C_{\text{O}}}{C_{\text{Al}}} = \frac{I_{\text{O}1s}^\infty(\alpha, \psi)}{I_{\text{Al}2p}^\infty(\alpha, \psi)} \cdot \frac{1}{S_{\text{O}1s/\text{Al}2p}(\alpha, \psi)} \quad (8)$$

where $I_{\text{O}1s}^\infty(\alpha, \psi)$, $I_{\text{Al}2p}^\infty(\alpha, \psi)$ and $S_{\text{O}1s/\text{Al}2p}(\alpha, \psi)$ denote the resolved O 1s PZL intensity, the resolved Al 2p PZL intensity and the corresponding experimentally determined RSF for

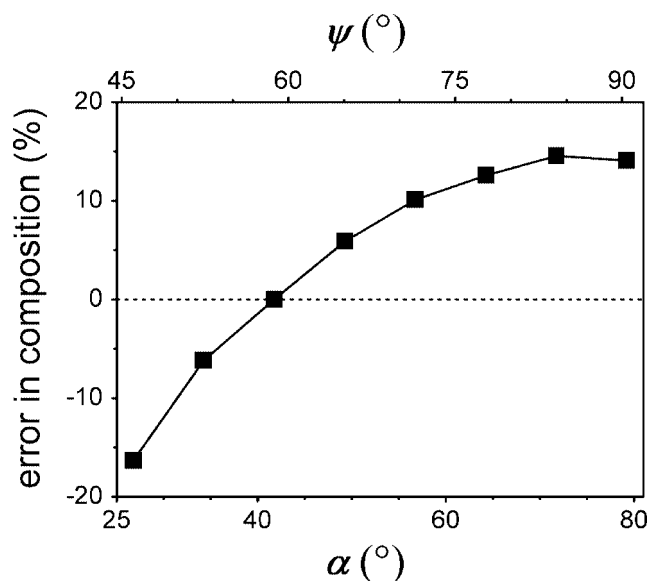


Figure 4. Error in the calculated composition (i.e. O/Al ratio) of $\alpha\text{-Al}_2\text{O}_3$ as a function of interdependent angles α (bottom x-axis) and ψ (top x-axis) that was introduced when adopting a single value for the relative sensitivity factor $S_{\text{O}1s/\text{Al}2p}$ ($\alpha = 41.8^\circ$, $\psi = 57.8^\circ$) (i.e. close to the magic angle of $\psi = 54.74^\circ$; see text). The straight line along the ordinate indicates the correct O/Al ratio for $\alpha\text{-Al}_2\text{O}_3$ of 3:2 that would be obtained when accounting for the effects of anisotropy of the photoionization cross-section and elastic scattering of the detected photoelectrons within the solid (see text for details).

a given set of angles α and ψ respectively. Figure 4 shows the percentage error introduced in the calculated values of the composition versus angles α and ψ when not taking into account the effects of anisotropy of the photoionization cross-section and elastic scattering, i.e. when adopting a single value for the RSF taken to be equal to the experimentally determined sensitivity factor $S_{\text{O}1s/\text{Al}2p}(\alpha = 41.8^\circ, \psi = 57.8^\circ)$ (i.e. close to the magic angle of $\psi = 54.74^\circ$). Clearly, when ignoring the effects of anisotropy of photoionization cross-section and elastic scattering, the magnitude of error induced in the compositional analysis of the ARXPS spectra recorded from binary solids in parallel data acquisition mode can be as high as 16%. Here, it should be noted that the contribution of elastic scattering to the introduced error is relatively small. By adopting values for the RSFs as a function of angles α and ψ determined experimentally from a reference solid of known composition, cumbersome corrections for the effects of the anisotropy of photoionization cross-section and elastic scattering can be avoided, e.g. for quantitative analysis of solids and thin-film structures of unknown composition and/or thickness.

CONCLUSIONS

For quantitative analysis of ARXPS spectra recorded in parallel data acquisition mode, it is essential to account for the anisotropies of the photoionization cross-sections of the concerned elements in the solid due to variation of angle ψ between the incident x-rays and the detected photoelectrons. The effect of elastic scattering on quantitative analysis of

the ARXPS spectra, as described by the effective asymmetry parameter β^{eff} and the correction factor Q , is relatively small (the effect being most pronounced in the grazing incidence angle range).

By adopting values for the RSFs of the concerned elements in the solids as a function of interdependent angles α and ψ , cumbersome corrections for the effects of the anisotropy of the photoionization cross-section and elastic scattering can be avoided, e.g. in the quantitative analysis of solids and thin-film structures of unknown thickness and/or composition. Values for the RSFs as a function of angles α and ψ , which incorporate the combined effects of the anisotropies of the photoionization cross-sections and elastic scattering, can be determined easily from ARXPS measurements of reference solids of known composition.

Acknowledgements

The authors are indebted to Prof. Dr Ir. E. J. Mittemeijer and Prof. Dr S. Hofmann for critical reading of the manuscript.

REFERENCES

1. Fadley CS. In *Electron Spectroscopy: Theory, Techniques and Applications*, Brundle CR, Baker AD (eds). Academic Press: London, 1978; Chapt. 1.
2. Fadley CS, Baird RJ, Seikhaus W, Novakov T, Bergstroem SAL. *J. Electron Spectrosc.* 1974; **4**: 93.
3. Jablonski A. *Surf. Interface Anal.* 1989; **14**: 659.
4. Jeurgens LPH, Sloof WG, Tichelaar FD, Mittemeijer EJ. *Surf. Sci.* 2002; **506**: 313.
5. Jeurgens LPH, Sloof WG, Borsboom CG, Tichelaar FD, Mittemeijer EJ. *Appl. Surf. Sci.* 2000; **161**: 139.
6. Jeurgens LPH. *Thesis*, Delft University of Technology, The Netherlands, 2001; 132.
7. Reilman RF, Msezane A, Manson ST. *J. Electron Spectrosc. Relat. Phenom.* 1976; **8**: 389.
8. Band M, Kharitonov YI, Trzhaskovskaja MB. *At. Data Nucl. Data Tables* 1979; **23**: 443.
9. Yeh J, Lindau I. *At. Data Nucl. Data Tables* 1985; **32**: 1.
10. Jablonski A, Zemek J. *Phys. Rev. B* 1993; **48**: 4799.
11. Jablonski A, Powell CJ. *Phys. Rev. B* 1994; **50**: 4739.
12. Jablonski A, Powell CJ. *Surf. Sci. Rep.* 2002; **47**: 33.
13. Jablonski A, Tilinin IS. *J. Electron Spectrosc. Relat. Phenom.* 1995; **74**: 207.
14. Jablonski A. *Phys. Rev. B* 1998; **58**: 16 470.
15. Chandrasekhar S. *Radiative Transfer*. Dover Publications: New York, 1960; Chapt. 5.
16. Seah MP, Gilmore IS. *Surf. Interface Anal.* 2001; **31**: 835.
17. Powell CJ. *Appl. Surf. Sci.* 1995; **89**: 141.
18. Wagner CD, Passoja DE, Hillery HF, Kinisky TG, Six HA, Jansen WT, Taylor JA. *J. Vac. Sci. Technol. A* 1982; **21**: 933.
19. Ching WY, Xu Y-N. *J. Am. Ceram. Soc.* 1994; **77**: 412.
20. Tanuma S, Powell CJ, Penn DR. *Surf. Interface Anal.* 1994; **21**: 165.
21. Jablonski A, Powell CJ. *NIST Electron Elastic-Scattering Cross-Section Database* (2nd edn), US Department of Commerce, Technology Administration (eds). NIST: Gaithersburg, MD, 2000.